Supporting information

Mass spectrometry spatial-omics on a single conductive slide

Stephanie T.P. Mezger[1,2,3], Alma M.A. Mingels[2,3], Otto Bekers[2,3], Ron M.A. Heeren[1] and Berta Cillero-Pastor[1*]

[1] Maastricht MultiModal Molecular Imaging (M4I) Institute, Division of Imaging Mass Spectrometry, Maastricht University, Universiteitssingel 50, 6229 ER Maastricht, The Netherlands; [2] Central Diagnostic Laboratory, Maastricht University Medical Center, P.O. Box 5800, 6202 AZ Maastricht, The Netherlands; [3] CARIM School for Cardiovascular diseases, Maastricht University, Universiteitssingel 50, 6229 ER Maastricht, The Netherlands

* corresponding author, email: b.cilleropastor@maastrichtuniversity.nl

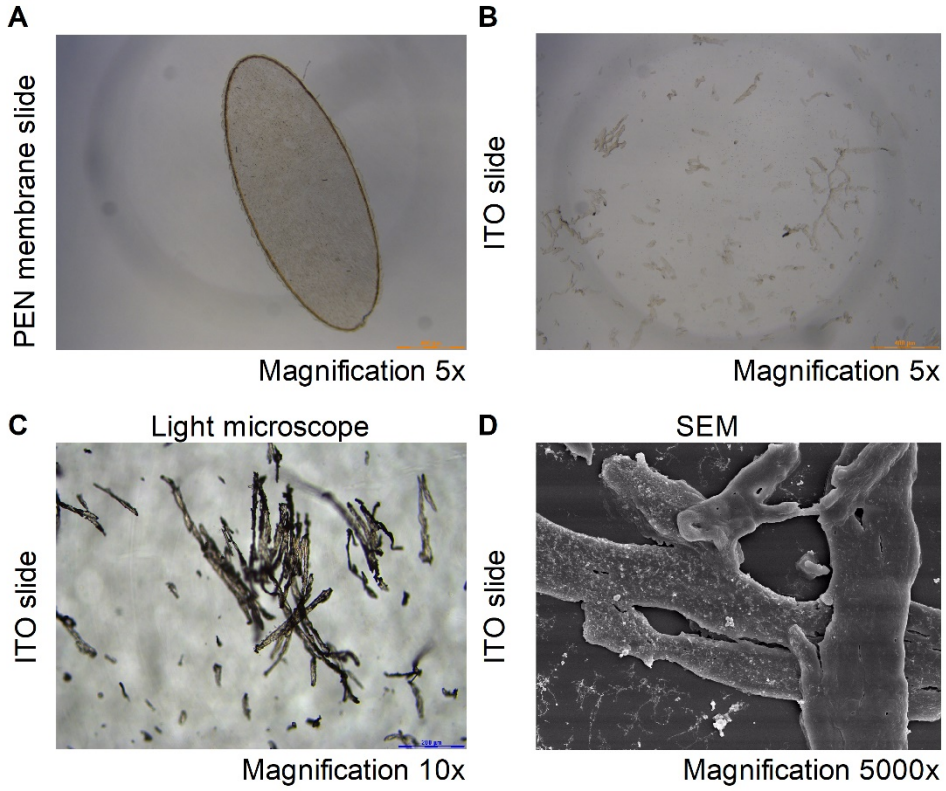

Supporting Figure S1. Images of the dissected tissue after laser capture microdissection (LMD). Tissue collected from (A) a PEN membrane slide and (B) an ITO slide, using a 5x magnification. The collected tissue from an ITO slide imaged (C) with a 10x magnification, and (D) using scanning electron microscopy (SEM) with a 5000x magnification.

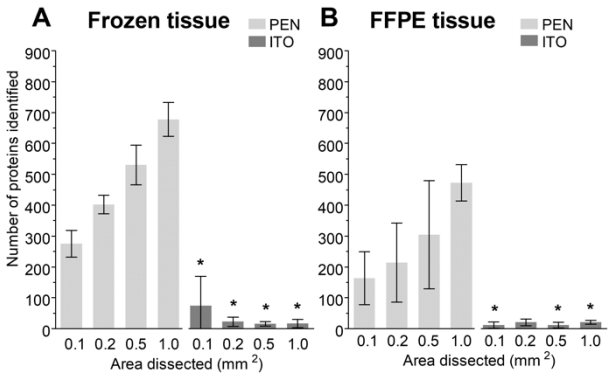

Supporting Figure S2. Proteins identified from PEN membrane and ITO slides after H&E staining, for (A) frozen tissue and (B) FFPE tissue. Data are presented as mean ± SD, * indicate $p<0.05$ when comparing equal areas from PEN membrane vs ITO slides.

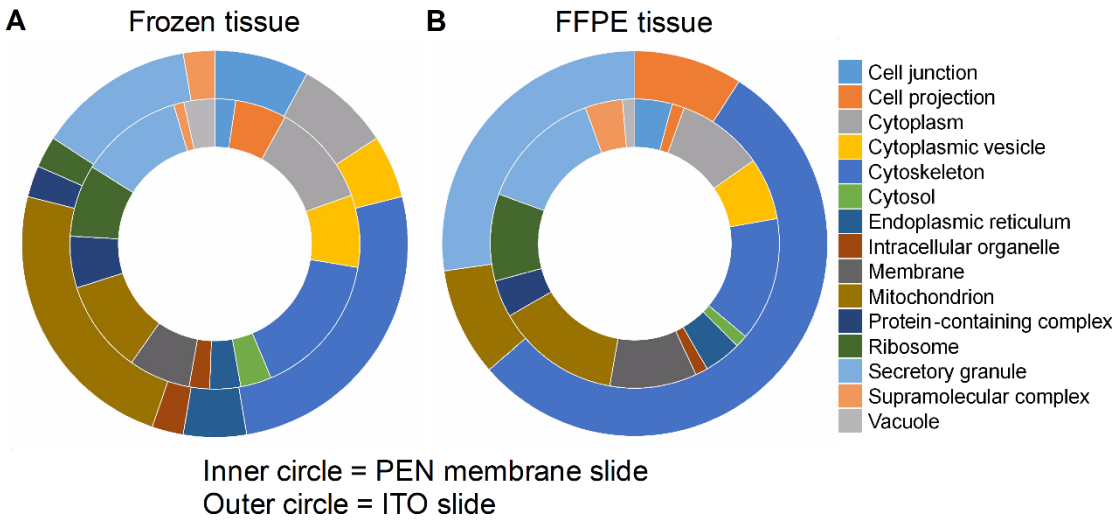

Supporting Figure S3. Categorized representation of the cellular components found after LMD on both frozen (A) and FFPE (B) tissue. For this analysis, all significant components (p<0.05) were considered. Information on the corresponding number of proteins per category can be found in Supporting Table S1.

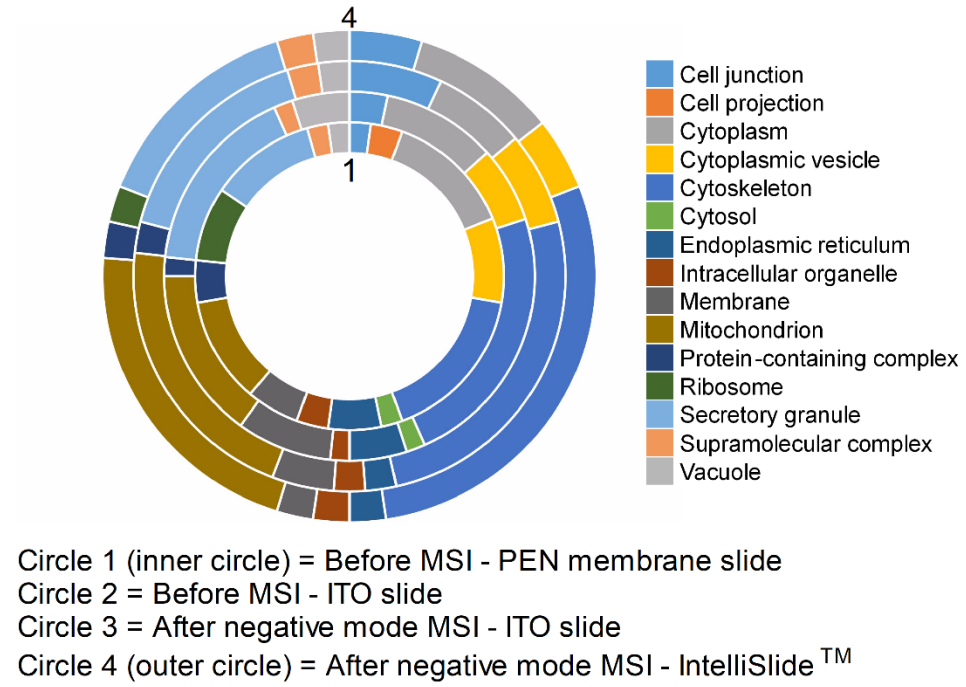

Supporting Figure S4. Cellular components found in frozen tissue before MALDI-MSI (circle 1; PEN membrane slide, 2; ITO slide) and after negative lipid MALDI-MSI (circle 3; ITO slide, 4; IntelliSlide^{TM}). All components with a p-value <0.05 were considered. The corresponding number of proteins per category can be found in Supporting Table S4.

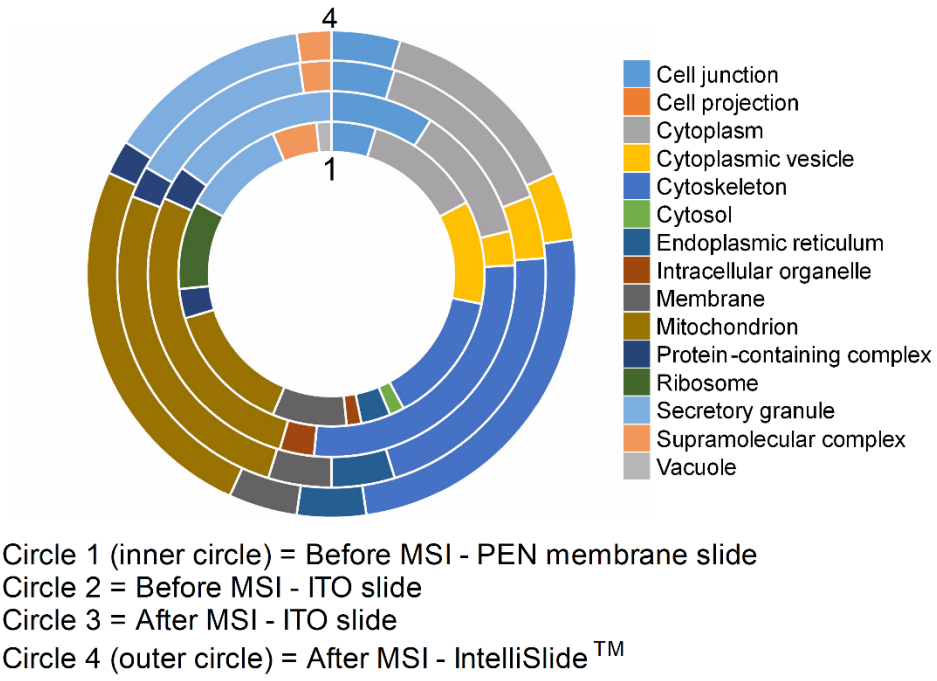

Supporting Figure S5. All cellular components found in FFPE tissue before (circle 1; PEN membrane slide, 2; ITO slide) and after metabolite MALDI-MSI (circle 3; ITO slide, 4; IntelliSlide™). Components with p-value<0.05 were considered. The corresponding number of proteins per category can be found in Supporting Table S5.

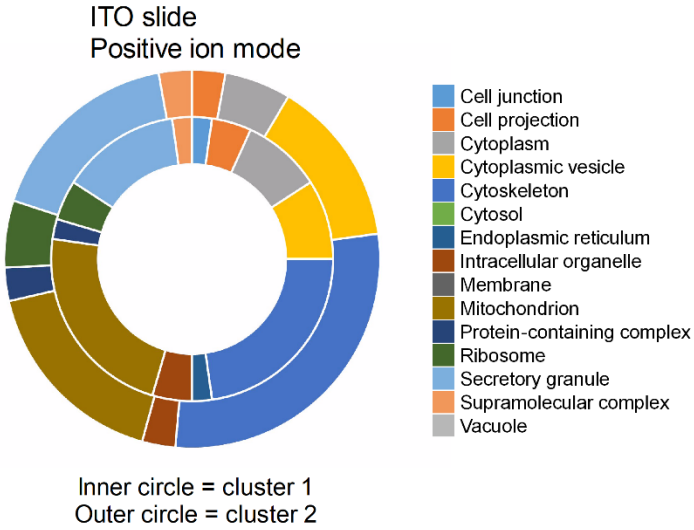

Supporting Figure S6. Cellular component analysis of the significant (p<0.05) components found in the two clusters dissected after positive lipid MALDI-MSI. The corresponding number of proteins per category can be found in Supporting Table S6.

Supporting Table S1. Number of cellular components and proteins after LMD on both frozen and FFPE tissue. The components were clustered and shown in alphabetical order. The column 'CC' contains the number of cellular components per category and 'protein' the number of proteins present in the category.

	Frozen tissue				FFPE tissue			
	PEN membrane slide		ITO slide		PEN membrane slide		ITO slide	
	CC (n=87)	protein	CC (n=38)	protein	CC (n=72)	protein	CC (n=11)	protein
Cell junction	2	66	3	16	3	54		
Cell projection	5	18			1	2	1	1
Cytoplasm	10	80	3	11	7	60		
Cytoplasmic vesicle	7	75	2	9	5	39		
Cytoskeleton	14	172	10	58	10	107	6	17
Cytosol	3	37			1	23		
Endoplasmic reticulum	3	47	2	7	3	25		
Intracellular organelle	2	14	1	1	1	5		
Membrane	6	32			7	35		
Mitochondrion	9	310	9	138	10	389	1	2
Protein-containing complex	5	16	1	3	3	15		
Ribosome	7	78	1	2	7	84		
Secretory granule	10	159	5	36	10	100	3	6
Supramolecular complex	1	3	1	2	3	11		
Vacuole	3	33			1	10		

Supporting Table S2. Top 10 cellular components for frozen and FFPE tissue comparing laser settings. The components were clustered and shown in alphabetical order.

	Frozen tissue		FFPE tissue	
Laser setting	A	B	A	B
Cell junction	x	x		
Cytoplasm	x	x	x	x
Cytoplasmic vesicle	x	x		
Cytoskeleton			x	x
Mitochondrion	x	x	x	x
Protein-containing complex				x
Secretory granule	x	x		x

Supporting Table S3. Top 10 cellular components from conductive slide before and after MALDI-MSI. The top 10 most significant components were clustered and shown in alphabetical order.

	Frozen tissue			FFPE Tissue		
	Before	After		Before	After	
	ITO	ITO	Intelli Slide	ITO	ITO	Intelli Slide
polarity		+/-	+/-		-	-
Cell junction	x				x	x
Cytoplasm	x	x/x	x/x	x		
Cytoplasmic vesicle	x		x/0			
Cytoskeleton		x/x	x/x	x	x	x
Mitochondrion	x	x/x	x/x	x	x	x
Protein-containing complex				x		
Secretory granule	x	0/x	x/x	x		

Supporting Table S4. Number of cellular components and proteins from frozen tissue before and after (positive or negative) lipid MALDI-MSI. The components were clustered and shown in alphabetical order. The column 'CC' contains the number of cellular components per category and 'protein' the number of proteins present in the category.

	Before MSI				After positive mode lipid MSI				After negative mode lipid MSI			
	PEN membrane		ITO		ITO		IntelliSlide™		ITO		IntelliSlide™	
	CC (n=90)	protein	CC (n=60)	protein	CC (n=40)	protein	CC (n=46)	protein	CC (n=43)	protein	CC (n=42)	protein
Cell junction	2	64	2	31					3	12	2	8
Cell projection	3	14			1	2	3	6				
Cytoplasm	12	96	6	33	2	9	2	9	3	12	4	14
Cytoplasmic vesicle	8	90	4	45	5	12	6	16	3	17	2	10
Cytoskeleton	15	154	14	96	10	51	10	50	11	68	12	66
Cytosol	2	38	1	6								
Endoplasmic reticulum	5	46	3	22	1	2	1	2	1	2	1	2
Intracellular organelle	3	16	1	5	1	1	1	1	1	3	1	1
Membrane	5	31	5	24	1	2	4	4	2	3	1	1
Mitochondrion	10	321	9	224	9	120	9	110	9	160	9	138
Protein-containing complex	4	16	1	3	1	2	1	1	1	2	1	2
Ribosome	7	92			2	4	2	4			1	2
Secretory granule	10	165	10	124	6	24	6	25	7	51	6	39
Supramolecular complex	2	8	1	2	1	2	1	2	1	2	1	2
Vacuole	2	23	3	24					1	5	1	4

Supporting Table S5. Number of cellular components and proteins from FFPE tissue before and after metabolite MALDI-MSI. The components were clustered and shown in alphabetical order. The column 'CC' contains the number of cellular components per category and 'protein' the number of proteins present in the category.

	Before MSI				After metabolite MSI			
	PEN membrane		ITO		ITO		IntelliSlideTM	
	CC (n=64)	protein	CC (n=33)	protein	CC (n=42)	protein	CC (n=44)	protein
Cell junction	3	46	3	9	2	26	2	26
Cell projection								
Cytoplasm	8	50	4	14	6	24	6	26
Cytoplasmic vesicle	7	49	1	5	2	16	2	16
Cytoskeleton	9	88	9	48	9	90	11	102
Cytosol	1	18						
Endoplasmic reticulum	2	21			2	12	2	12
Intracellular organelle	1	7	1	1				
Membrane	5	26			2	5	2	5
Mitochondrion	9	366	9	145	11	280	11	293
Protein-containing complex	2	7	1	3	1	3	1	3
Ribosome	6	65						
Secretory granule	7	85	5	29	6	55	6	56
Supramolecular complex	3	9			1	2	1	2
Vacuole	1	10						

Supporting Table S6: Number of cellular components and proteins from cluster 1 and 2 after positive lipid MALDI-MSI. The components were clustered and shown in alphabetical order. The column 'CC' contains the number of cellular components per category and 'protein' the number of proteins present in the category.

	Cluster 1		Cluster 2	
	CC (n=44)	protein	CC (n=35)	protein
Cell junction	1	5		
Cell projection	2	3	1	1
Cytoplasm	4	13	2	8
Cytoplasmic vesicle	4	9	5	11
Cytoskeleton	10	49	10	47
Cytosol				
Endoplasmic reticulum	1	2		
Intracellular organelle	2	3	1	1
Membrane				
Mitochondrion	10	113	6	52
Protein-containing complex	1	2	1	1
Ribosome	2	4	2	4
Secretory granule	6	23	6	24
Supramolecular complex	1	2	1	2
Vacuole				

Supporting Table S7. Pathway analysis from clusters 1 and 2 after positive lipid MALDI-MSI. All significant pathways (p<0.05) were included and displayed in alphabetical order.

Common pathways, n=41	**Specific for cluster 1, n=29**	**Specific for cluster 2, n=33**
AUF1 (hnRNP D0) binds and destabilizes mRNA	Activation of caspases through apoptosome-mediated cleavage	Assembly of the HIV virion
Beta oxidation of lauroyl-CoA to decanoyl-CoA-CoA	Acyl chain remodeling of CL	Association of licensing factors with the pre-replicative complex
Binding and uptake of ligands by scavenger receptors	Amino acid synthesis and interconversion (transamination)	Cell-extracellular matrix interactions
CHL1 interactions	Apoptotic factor-mediated response	Constitutive Signaling by NOTCH1 HD domain mutants
Citric acid cycle (TCA cycle)	Beta oxidation of decanoyl-CoA to octanoyl-CoA-CoA	Diseases of carbohydrate metabolism
Creatine metabolism	Beta oxidation of hexanoyl-CoA to butanoyl-CoA	Disorders of transmembrane transporters
Downregulation of ERBB4 signaling	Beta oxidation of octanoyl-CoA to hexanoyl-CoA	Downregulation of ERBB2:ERBB3 signaling
Erythrocytes take up carbon dioxide and release oxygen	Branched-chain amino acid catabolism	Glycogen breakdown (glycogenolysis)
Erythrocytes take up oxygen and release carbon dioxide	Cellular responses to stress	Glycogen storage diseases
Gluconeogenesis	Complex I biogenesis	Glycogen synthesis
Glucose metabolism	Cytochrome c-mediated apoptotic response	Hemostasis
Glycolysis	Detoxification of reactive oxygen Species	IRAK2 mediated activation of TAK1 complex
Lipid digestion, mobilization, and transport	Fatty acid, triacylglycerol, and ketone body metabolism	IRAK2 mediated activation of TAK1 complex upon TLR7/8 or 9 stimulation
Metabolism	Fructose metabolism	MAP3K8 (TPL2)-dependent MAPK1/3 activation
Metabolism of amino acids and derivatives	Glyoxylate metabolism and glycine degradation	Membrane binding and targeting of GAG proteins
Metabolism of carbohydrates	Histidine, lysine, phenylalanine, tyrosine, proline and tryptophan catabolism	Membrane trafficking
Metabolism of polyamines	Hormone-sensitive lipase (HSL)-mediated triacylglycerol hydrolysis	Myoclonic epilepsy of Lafora
mitochondrial fatty acid beta-oxidation of saturated fatty acids	Ion homeostasis	NF-kB is activated and signals survival

mitochondrial fatty acid beta-oxidation of unsaturated fatty acids	Ketone body metabolism	NRIF signals cell death from the nucleus
Mitochondrial protein import	Lysine catabolism	p75NTR recruits signaling complexes
Mitophagy	Metabolism of lipids and lipoproteins	p75NTR signals via NF-kB
Muscle contraction	Methionine salvage pathway	Receptor-ligand binding initiates the second proteolytic cleavage of Notch receptor
O2/CO2 exchange in erythrocytes	Mitochondrial fatty acid Beta-Oxidation	Recycling of bile acids and salts
Pink/Parkin mediated mitophagy	Neurotransmitter clearance in the synaptic cleft	Reduction of cytosolic Ca++ levels
Platelet activation, signaling and aggregation	Pregnenolone biosynthesis	Regulation of innate immune responses to cytosolic DNA
Platelet degranulation	Regulation of pyruvate dehydrogenase (PDH) complex	Regulation of PLK1 activity at G2/M transition
PTK6 regulates RTKs and their effectors AKT1 and DOK1	Signaling by retinoic acid	Signaling by NOTCH1 HD domain mutants in cancer
Pyruvate metabolism	Synthesis of ketone bodies	Spry regulation of FGF signaling
Pyruvate metabolism and citric acid (TCA) cycle	Transcriptional regulation by TP53	Synthesis and processing of GAG, GAGPOL polyproteins
Regulation of cytoskeletal remodeling and cell spreading by IPP complex components		TGF-beta receptor signaling in EMT (epithelial to mesenchymal transition)
Regulation of mRNA stability by proteins that bind AU-rich elements		TRAF6 mediated induction of TAK1 complex
Respiratory electron transport		Translesion synthesis by REV1
Respiratory electron transport, ATP synthesis by chemiosmotic coupling, and heat production by uncoupling proteins.		Transport of organic anions
Response to elevated platelet cytosolic Ca2+		
Scavenging of heme from plasma		
SLC transporter disorders		
Striated muscle contraction		
The citric acid (TCA) cycle and respiratory electron transport		
TP53 regulates metabolic genes		
Translocation of GLUT4 to the plasma membrane		
Vesicle-mediated transport		